J. Synchrotron Rad. (1998). **5**, 1346–1356

D2AM, a Beamline with a High-Intensity Point-Focusing Fixed-Exit Monochromator for Multiwavelength Anomalous Diffraction Experiments

J.-L. Ferrer,[a] J.-P. Simon,[b] J.-F. Bérar,[c] B. Caillot,[c] E. Fanchon,[d] O. Kaïkati,[a] S. Arnaud,[c] M. Guidotti,[a] M. Pirocchi[a] and M. Roth[a]*

[a]Laboratoire de Cristallographie et Cristallogénèse des Protéines (LCCP), Institut de Biologie Structurale Jean-Pierre Ebel, 41 Avenue des Martyrs, 38027 Grenoble CEDEX 1, France, [b]Laboratoire de Thermodynamique et Physico-Chimie Métallurgiques, Institut National Polytechnique de Grenoble (LTPCM/INPG), Domaine Universitaire, BP 75, 38402 Saint-Martin d'Hères CEDEX, France, [c]Laboratoire de Cristallographie, Centre National de la Recherche Scientifique (LCG/CNRS), 25 Avenue des Martyrs, BP 166, 38042 Grenoble CEDEX 09, France, and [d]Laboratoire de Cristallographie Macromoléculaire (LCM), Institut de Biologie Structurale Jean-Pierre Ebel, 41 Avenue des Martyrs, 38027 Grenoble CEDEX 1, France. E-mail: roth@lccp.ibs.fr

(*Received 13 June 1997; accepted 19 March 1998*)

D2AM is a french CRG beamline installed at the ESRF (European Synchrotron Radiation Facility) in Grenoble, with half of the time dedicated to biological macromolecule crystallography and half to materials science studies (diffraction, wide-angle and small-angle scattering). It is constructed at the front-end BM02 of the ESRF storage ring, using the X-ray beam from a 0.8 T bending magnet. D2AM entered into routine operation at the end of 1994, and is used either for single-wavelength or for multiwavelength anomalous diffraction studies. The beam is monochromated by an Si[111] two-crystal monochromator with a resolution of about 2×10^{-4}. The first crystal is water cooled. The X-ray photon energy covers the range between 6.5 keV ($\lambda \simeq 1.9$ Å) and 17 keV ($\lambda \simeq 0.7$ Å), a domain of energy with many *K* or *L* absorption edges of heavy atoms of interest for biological macromolecules studies and in materials science. The X-ray beam is focused in the vertical plane by two long curved mirrors and in the horizontal plane by the second crystal of the monochromator which is given an adjustable sagittal curvature. A spot size of 0.3×0.1 mm (FWHM) is measured at the sample position. Both mirrors are cut out of a 6"-diameter 1.1 m-long Si single crystal, polished and coated with a 400 Å Pt thin film. The rugosity is better than 4 Å r.m.s. and the longitudinal slope error is better than 5×10^{-6} rad r.m.s. The first mirror is water cooled, the second is not. The beam intensity on the sample is about 10^{11} photon s^{-1} on a 0.3×0.3 mm focus area at 100 mA in the storage ring of the ESRF. The harmonic rejection ratio obtained with the two mirrors is better than 10^{-5} for $\lambda/3$. The combined optical system, mirror/monochromating-crystals/mirror, used on D2AM constitutes altogether a high-intensity point-focusing fixed-exit monochromator, which has the additional property that the energy resolution is not dependent on the beam divergence in use. Its stability and resolution are perfectly adapted to multiwavelength anomalous diffraction studies. The alignment of the mirrors and the monochromator is fully automated, taking 5 min, with the exception of the adjustment of the sagittal focusing. During multiwavelength diffraction experiments the wavelength is changed by a fast single monochromator rotation. Neither realignment of the mirrors nor readjustment of the beam focusing are necessary. The stability and reproducibility of the selected X-ray photon energy is better than 0.5 eV.

Keywords: X-ray beamlines; X-ray monochromators; anomalous diffraction; focusing mirrors; sagittal focusing.

1. Introduction – design of the beamline

The beamline D2AM has been primarily designed for multiwavelength anomalous diffraction or scattering experiments, including small-angle scattering, in materials science and biological macromolecule crystallography. Anomalous diffraction or scattering experiments are most often carried out by small-step scanning of the absorption edge of a given heavy atom, with very frequent wavelength changes. In protein crystallography, for example, these

Table 1
Beamline general data.

Magnetic field in bending magnet	0.8 T
Critical energy of produced X-ray beam	19.2 keV
Maximum horizontal divergence at 0.8 T	3 mrad
Size of beam at source on storage ring	FWHM < 0.3 mm
Total energy of beam per mrad of horizontal fan	~70 W at 100 mA

X-ray energy		25 keV	5 keV
Vertical beam divergence at source	FWHM	0.11 mrad	0.25 mrad
Vertical size of beam at 25 m	FWHM	3.07 mm	6.54 mm
	FW at 0.1 m	5.8 mm	9.3 mm
Critical angle of total reflection with Pt coating		3.2 mrad	16 mrad
Size of beam on inclined mirror	FWHM	0.96 m	0.41 m
Beam intensity loss on 1.1 m-long mirror		~10%	~0

changes can be as frequent as one every few seconds. Therefore it was decided to realise an X-ray optics allowing very fast and accurate wavelength changes without changing the beam position at the sample.

The beamline is built on a bending-magnet beam port, giving a white beam with almost constant intensity between 5 and 40 keV. Some of the main parameters of the beamline are given in Table 1. The beam divergence is of the order of 0.1–0.2 mrad in the vertical plane depending on the wavelength. In the horizontal plane, the beam is limited to 3 mrad, but the incoming-beam horizontal divergence, which is effectively used in most of the experiments, is usually less than 3 mrad. The distance from the source to the front-end exit is ~24 m because of the thick radioprotective concrete shielding surrounding the ESRF storage ring. Refocusing the outgoing beam onto the sample is an absolute necessity in order to avoid spoiling the high intensity of the source.

The instrument was built according to the following guidelines: (i) point focusing of the beam on the crystal, with 3/1 demagnification; (ii) fixed focusing distance and fixed sample position, (iii) high energy resolution, 2–5 eV; (iv) high scattering vector resolution, 2×10^{-3} Å^{-1}; (v) accessible wavelength range, 0.5–2.5 Å (25–5 keV); (vi) high rate of harmonic rejection, better than 10^{-4}.

The high energy resolution is dictated by the fine structure of the absorption edges and the high scattering vector resolution by the diffraction conditions (protein crystal lattice parameters as large as 300 Å, for example, or small-angle scattering). A fixed focusing distance and fixed beam exit require that the focusing devices (mirror and monochromator crystal) have adjustable curvature, and that pairs of reflecting optical elements must be used: two mirrors and two monochromator crystals (Simon *et al.*, 1992). Fig. 1 shows a schematic representation of the beam focusing and beamline layout. The two-crystal monochromator is installed between two cylindrical focusing mirrors, the distance between the mirror and monochromator being as short as possible. The mirrors reflect the beam at grazing incidence.

The function of the first mirror, located upstream and curved cylindrically in the vertical plane, is to absorb a large part of the incoming energy, by absorbing the non-reflected high-energy X-rays, and to cancel out the vertical

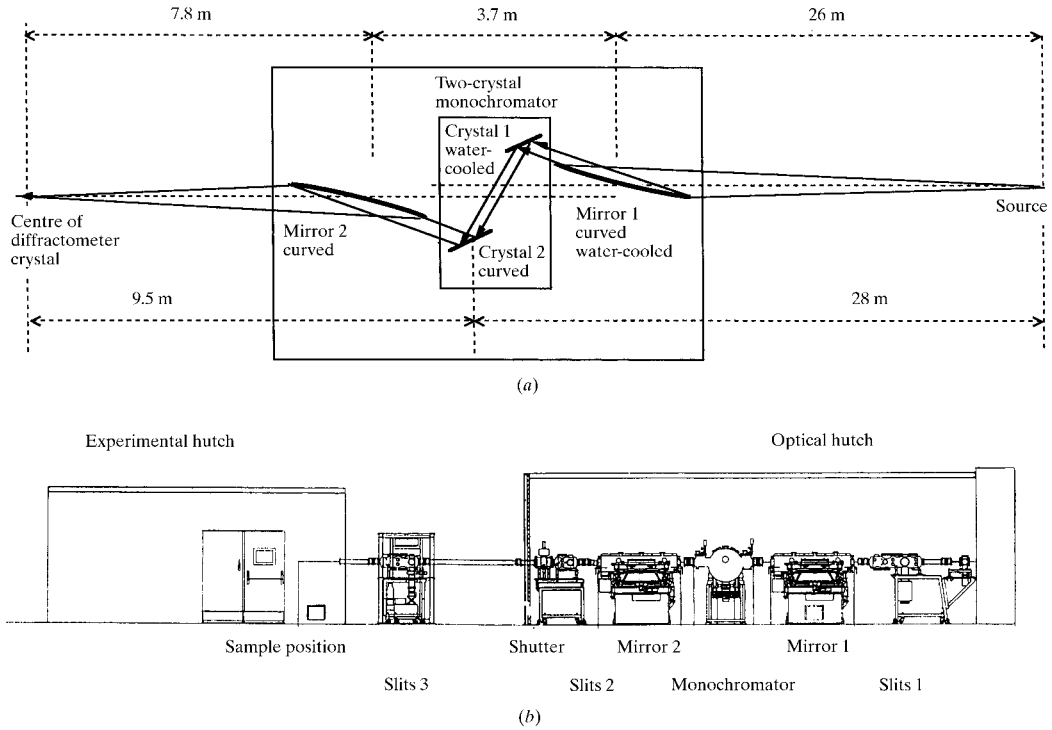

Figure 1
Schematic representation of (*a*) the beam focusing and (*b*) the layout of the beamline D2AM.

divergence of the beam after reflection. The second mirror, which is identical to the first mirror and is placed downstream in a position symmetrical to the first with respect to the monochromator, is used for focusing and directing the beam coming out of the monochromator onto the sample. High-rate harmonic rejection is achieved by the two mirrors.

One of the key properties of this optical system is that the beam between the mirrors has vanishing vertical divergence. Therefore, one can use, in the monochromator, flat parallel perfect single crystals which will reflect the beam on its full vertical height. The first crystal has to be cooled because it absorbs most of the energy remaining in the beam. With flat crystals, the design of the cooling of the first crystal is simpler and the second crystal can be used for horizontal focusing by cylindrical sagittal bending. The two-crystal monochromator is not a fixed-beam-exit monochromator. It is the mirrors–monochromator system which is a fixed-exit optical system.

1.1. *Advantages of the two-mirror two-crystal-monochromator optical system*

Considering a given energy resolution, this focusing system gives ideally the highest intensity possible on a point sample from a divergent beam emitted by a point source. The energy resolution is not dependent on the incoming beam divergence and can be adjusted by changing the mirror curvature. Its minimum value is determined by the Darwin width of the monochromator crystals. The intensity is at its highest because the full divergence of the incoming beam can be used. In addition, horizontal beam focusing by a curved crystal is not hampered by the unavoidable limitation of focusing by a toroidal mirror, where, even with a more than 1 m-long mirror, the full beam cannot be reflected, and part of the beam hits the entrance face.

There are, in addition, a number of other interesting features. The system gives very high flexibility for adjusting the direction of the outgoing beam. By tilting the second mirror around a horizontal axis perpendicular to the mean beam direction, and the curved crystal around a horizontal axis parallel to the mean beam direction, the direction of the outgoing beam can be adjusted vertically and horizontally, respectively, with very high precision and without any coupling between the direction of the beam and neither the wavelength of the beam nor the energy resolution. This allows beam-position servo-monitoring, which will increase the stability of the intensity on the crystal.

High harmonic rejection is achieved without detuning the two crystals of the monochromator. Combining harmonic rejection by crystal detuning and beam focusing by sagittal curvature of one of the crystals is, in practice, barely possible. No beam polarization monitoring is required because almost full beam is used in the vertical direction; the average beam polarization is constant.

The major technical difficulty which has to be properly solved with this optical system is the control of the curvature and of the alignment of the second crystal. This will be described in more detail later in this paper.

The high flexibility of this optical system has its counterpart which is the complexity of setting up the ensemble. However, most of the beam and optics parameters can be easily controlled. Beamline monitoring will be described later in the paper. Presently, given the wavelength, all beam alignment operations are performed automatically in 5 min with the exception of horizontal focusing.

1.2. *Running an anomalous dispersion multiwavelength experiment*

Full beamline adjustments are not made during the course of an anomalous diffraction experiment performed in the vicinity of a given absorption edge. Once the beam is adjusted and focused onto the sample at the nominal wavelength value of the absorption edge, changing the X-ray wavelength within $\pm 10\%$ of the average value is performed by a simple rotation of the central monochromator rotation axis, without any other crystal or mirror readjustment. The width of this energy range is limited by the defocusing of the beam. In case of a bad alignment of the curved crystal, it may happen that a small horizontal shift of the beam occurs during the wavelength change. This can be detected by a beam-position monitor and minimized by good alignment of the curved crystal. This shift can also result from a global misalignment of the beamline, *i.e.* from the source, the crystals in the monochromator and the centre of the diffractometer.

2. Description of the beamline

2.1. *Mirrors*

The first mirror receives the white beam and it is therefore submitted to high ionization radiation damage and a heat load which can be higher than 100–200 W. These conditions lead us to choose silicon as the best appropriate material. Contrary to glass and amorphous silica, it is not very sensitive to radiation damage, has very favourable thermal properties, low thermal expansion coefficient (2.55×10^{-6} K^{-1} at room temperature) and good thermal conductivity (149 W m^{-1} K^{-1} at room temperature), and is not very expensive. The thermal load on this mirror is such that, in a vacuum without any cooling but radiative cooling, the temperature would rise to 423 K with a time constant of several hours. It is therefore necessary to cool the mirror in order to keep its temperature near room temperature. In order to minimize the curvature induced by thermal gradients resulting from the cooling, the heat is evacuated on the side of the mirror, through narrow ribs dipping in two long and narrow vessels filled with liquid Ga eutectic and cooled by water circulation (Roth *et al.*, 1992). Thermomechanical three-dimensional simulations (ANSYS, 1991) showed that the bulk remains quasi-isothermal and that the curvature of the reflecting surface due to thermal effects is negligible compared with the curvature used for beam focusing. Because of practical aspects of this cooling

system, the mirror reflects the beam upwards. The first mirror is installed at 26 m from the bending-magnet source in ultrahigh vacuum ($<10^{-8}$ mbar), the second mirror, at 3.7 m downstream, after the monochromator in a high-vacuum vessel ($<10^{-6}$ mbar) without a cooling system because it is not submitted to any heat load. It is located at 7.8 m from the sample and reflects the beam downwards.

The two mirrors were cut out of the same 6"-diameter 1.1 m-long Si single crystal and polished by REOSC (91200 Massy, France). The polished reflecting surface of the mirrors is coated with a 400 Å-thick film of platinum. The residual roughness of the surface has been estimated to be ~2–4 Å r.m.s. using standard samples as references. An overall longitudinal r.m.s. slope error lower than 5 µrad has been measured. The residual curvature radius of the reflecting surface is higher than 80 km. The reflecting surface has an effective length of 1.1 m and a width of 0.09 m which allows the use of an incoming beam of up to 3 mrad horizontal divergence.

2.1.1. *Bending and inclining the mirrors*. Bending of the mirrors is produced by applying equal and opposite torques at both ends of the mirrors. The system is represented schematically in Fig. 2. The bender and mirror holder are mechanically decoupled from the vacuum vessel to avoid vibrations originating in other parts of the beamline. The mirrors sit on two ~1 m-distant cylinders which are carried by an inclinable plateau. The rotation of the plateau around a horizontal axis perpendicular to the beam allows one to adjust the angle of incidence of the beam on the mirror between 0.15 and 0.75°. The plateau can also be translated vertically in order to adjust the position of the mirror to the altitude of either the incoming beam (mirror 1) or the sample altitude (mirror 2). Two other cylinders, about 5 cm apart from the supporting cylinders, press from the top onto the mirrors producing the bending torques at each end. The strength of the force applied by these cylinders is adjusted by shifting heavy mobile counterweights. The mechanics for inclination, translation and bending of the mirrors are located outside the vacuum vessels and are fully motorized. Two static systems of counterweights are installed under the mirrors to compensate for the weight of the mirror. They reduce strongly the curvature due to gravity. A theoretical calculation shows that, without counterweighting, the average slope error due to gravity curvature would be almost 50 µrad. With two counterweights, an optimal solution is found when the counterweights are placed at 0.3026 and 0.6974 of the mirror length and the applied force is 39% of the full weight per counterweight, the slope error then being reduced to 0.69 µrad. The radii of curvature range from 4 to 20 km and 1.2 to 6 km for mirrors 1 and 2, respectively, depending on the angle of incidence of the beam, the focusing distance being equal to 26 m and 7.8 m, respectively. A focal spot on the sample of ~0.1 mm FWHM in height is currently obtained with this focusing system.

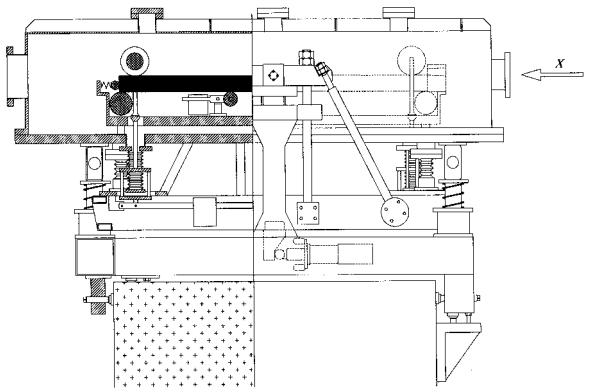

Figure 2
Drawing of the mirror holder and vessel. Right-hand side: external view of the vacuum vessel, also showing the lower part of the oscillating table by which the inclination of the mirror is adjusted from the outside. Left-hand side: cross section of the vessel. The lower part (outside vessel) and upper part (inside vessel) of the oscillation table is shown, as well as the bending mechanism with the two cylinders on both ends of the mirror by which the bending torques are applied.

2.1.2. *Reflectivity and harmonic filtering*. The reflectivity of Pt is shown in Fig. 3(*a*) as a function of X-ray energy for different beam incidence angles $i \simeq p\theta$, where θ is the critical angle of total reflection and p = 0.0, 0.4, 0.8 and 1. These curves were calculated using f' and f'' shown in Fig. 3(*b*) deduced from the fluorescence of a thin Pt foil. As can be seen, the reflectivity is markedly reduced with respect to 1 at the critical angle at any energy. This effect is due to the absorption of X-rays by Pt and is especially strong in the vicinity of the Pt absorption-edge energy. A drop in intensity of about 2 to 3 can be observed at the maximum of f''. Highest harmonic rejection (*i.e.* lowest reflectivity for harmonics) is obtained with highest angles of incidence i. This can be quantified by observing that, beyond the domain of total reflection, the reflectivity decreases asymptotically as (James, 1982)

$$R \simeq (1/16)(\theta/i)^4.$$

The critical angle, θ_n, of total reflection of the harmonic n is related to θ by

$$\theta_n \simeq \theta/n.$$

The reflectivity of the Pt-coated mirror for this harmonic is of the order of $(2pn)^{-4}$, or $(2pn)^{-8}$ with two mirrors. As seen in Fig. 3(*c*), a good reflectivity is obtained at almost all energies with a beam incidence angle i of the order of 0.75θ. For obtaining high harmonic rejection at a given energy, it is thus necessary to adjust the inclination of the mirror at this incidence. With n = 3 and p = 0.75, the rate of third-harmonic rejection is thus of the order of 6×10^{-6}.

Remark on rugosity and slope error. In Fig. 3(*d*), showing the calculated asymptotic reflectivity of a Pt-coated mirror, it can be seen that the rugosity of the mirror enhances the harmonic filtering. The influence of the rugosity was estimated by multiplying the ideal reflectivity R by the attenuation factor $\exp[-(4\pi\sigma ni/\lambda)^2]$ according to Bilderback (1981). Because of the very small r.m.s. rugosity, σ, of

the mirrors, this attenuation factor is close to unity as far as the reflectivity of the fundamental wavelength, λ, is concerned. The trade-off between minimal rugosity and minimal slope error, which must often be made when polishing a mirror, should therefore be made in favour of minimal slope error because the slope error constitutes one important limit to optimal beam focusing.

2.1.3. *Energy resolution and mirror curvature*. The curvature of the first mirror has to be adjusted to obtain a parallel beam on the first crystal of the monochromator. Because the vertical divergence of the beam after the first mirror is not directly measurable, the curvature of the mirror has been calibrated by minimizing the energy resolution of the monochromated beam. The energy resolution was determined by the width of the peak of the fluorescence of Ir at the Ir L_{III} absorption edge measured as a function of X-ray energy. The influence of the mirror curvature on the energy resolution can be seen clearly in Fig. 4.

2.2. *Monochromator*

The wavelength selection is performed by a two-crystal monochromator. Both crystals of this monochromator operate in a vertical diffraction plane. The first crystal is flat and the second one is bent for sagittal focusing. With Si[111] crystals, the optimal wavelength range is in the range 0.8–1.4 Å. Outside this domain, the intensity of the beam falls off rather rapidly.

The first crystal of the monochromator is placed approximately midway between the two mirrors, on the main rotation axis of the monochromator, which is horizontal and perpendicular to the beam. The second crystal is parallel to the first one and rotates jointly on the same axis. With two orthogonal translations X and Y, this crystal is placed downstream at the correct distance from crystal 1, for directing correctly the beam towards the second mirror. The crystal-to-crystal distance is short, varying between 5 and 15 cm. The difference in altitude between the beam

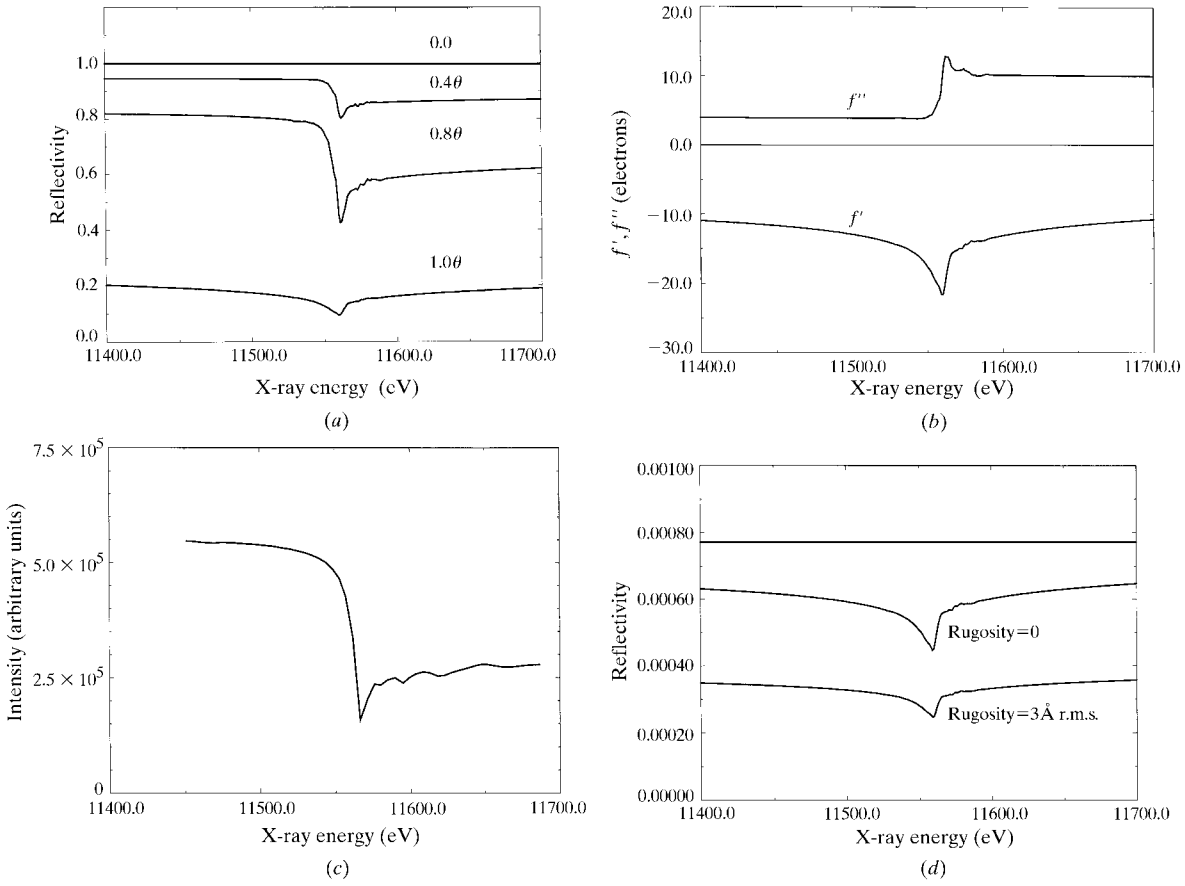

Figure 3
Reflectivity of Pt mirrors near the Pt absorption edge. (*a*) Theoretical reflectivity of a Pt mirror calculated (James, 1982) with the f' and f'' data of (*b*), at several beam incidences $p\theta$, where θ is the ideal total reflection critical angle calculated at the wavelength corresponding to the Pt L_{III} absorption edge, λ = 1.0723 Å, and p = 0.0, 0.4, 0.8, 1. (*b*) f' and f'' of Pt as a function of energy, deduced from the fluorescence of a Pt foil using the method of Hendrickson *et al.* (1988). (*c*) Intensity of the beam at D2AM after reflection on the Pt-coated mirrors, as a function of energy, at a fixed beam incidence on the mirrors equal to 0.75θ. This curve compares almost to the theoretical curve shown in (*a*) for p = 0.8. (*d*) Same as (*a*), at incidence 3θ. Upper curve: ideal reflectivity; lower curves: reflectivity calculated with the real f' and f'' values and 0 and 3 Å r.m.s. rugosity of the mirrors, respectively. These curves demonstrate the efficiency of the mirrors for λ/3 harmonic filtering, enhanced by rugosity.

before the first crystal and after the second crystal is about 5 cm. The whole monochromator is translated vertically in order to follow shifts of the beam produced by inclination changes of the first mirror. The Bragg angle of both crystals is adjusted by the main rotation of the monochromator (rotation β). The rotation is driven by a stepping motor with a resolution of 0.5×10^{-4} deg (∼1") and is encoded by a Heydenhain ERO725 encoder with a resolution of 5×10^{-4} deg. All motors of the monochromator are in a vacuum at $\sim 10^{-6}$ mbar and are cooled by water.

2.2.1. *First crystal.* The first crystal has to be cooled because of the incident thermal load of ∼100 W. The cooling system is presently constituted by a water box on which the crystal, an 8 mm-thick 60 × 80 mm flat platelet of Si, is firmly held, with a thin film of liquid gallium eutectic in between for good thermal exchange. The water circulates by pure gravitation from an upper reservoir in order to avoid vibrations from standard water supplies or mechanical circulators. The curvature of the crystal due to differential thermal expansion of the crystal between front and back produces an increase in beam divergence of about $\gamma_1 \simeq 2l/R_g$, where l is the length of the crystal along the beam direction and R_g is the radius of curvature. Because the second crystal diffracts only that part of the beam having the correct incidence and wavelength, this thermal deformation produces a loss of beam intensity of the order of $\omega_D/(\omega_D{}^2 + \gamma_1{}^2)^{1/2}$, where ω_D is the Darwin width of the Bragg reflection ($\omega_D \simeq$ 10–40 μrad for an Si[111] reflection). If crystal 1 is curved, only part of its surface is effectively used for beam diffraction.

Instead of using a thick Si plate, a bilayer technique was also tried (Roth *et al.*, 1992; Ferrer *et al.*, 1995). Differential thermal expansion between front and back can be theoretically exactly compensated, independently of the thermal load, by depositing on the back of the Si crystal a thin film of a material having a large thermal expansion (Roth *et al.*, 1992). The model was tested by using a 2 mm-thick Si crystal with a coating of ∼5 μm pure Ni on the back (Ferrer *et al.*, 1995). It was shown that this bilayer system can be produced, by electrochemical Ni deposition, without significant initial slope error at room temperature, that a rather low curvature of the crystal can be maintained during white X-ray beam exposure, and that the curvature can be varied by changing the temperature of the cooling water. Nevertheless, the tests were not continued because of the high sensitivity of the thin crystal to capillary forces due to the liquid gallium film, on which the crystal is placed, acting as a new uncontrolled and temperature-sensitive source of crystal curvature.

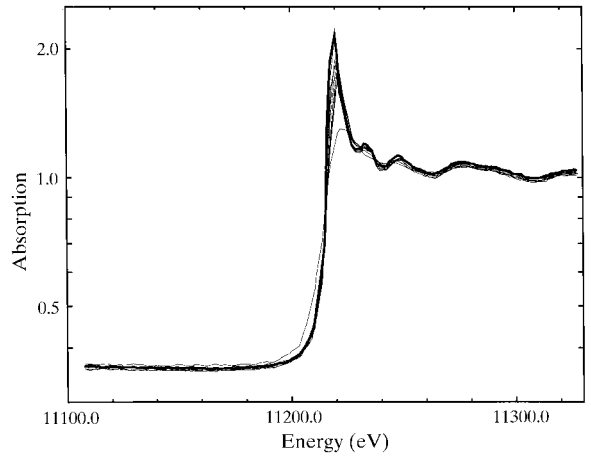

Figure 4
Ir L_{III} absorption edge, E = 11212 eV, recorded at various curvatures of the first mirror. The best energy resolution, reached at the maximum of the white line, can be estimated to be equal or better than 2 eV (also see Fig. 11).

2.2.2. *Second crystal.* This crystal is bent around an axis parallel to the average beam direction. Heat-load effects due to the incident beam are negligible. The sagittal bending produces an important longitudinal curvature of this crystal, the anticlastic curvature, in the diffraction plane. The effect on the beam intensity is the same as for thermal curvature of crystal 1, except that it is at least two orders of magnitude larger; the two curvatures cannot compensate. Reducing the anticlastic curvature by two or three orders of magnitude is therefore an absolute necessity for obtaining a high intensity. Using three-dimensional mechanical modelling (ANSYS, 1991), we have seen that, by using a specific design of the profile of the back of the bent crystal plate, a sagittal bending free of anticlastic curvature at the centre could be achievable. Unfortunately the machining of this profile in a silicon single crystal seems to be barely possible with an accuracy of the order of 10 μm which is required by the model. We therefore use the classical solution of a thin silicon crystal with ribs on the back (Sparks *et al.*, 1982). Details of the crystal holder and bender are shown in Fig. 5. The crystal has an area of ∼50 × 100 mm, the ribs are 0.4 mm thick and 7 mm high, the gap between the ribs is 0.8 mm, and the crystal is glued by Wood metal at both ends on the holder. With this device, we are able to produce a focus spot on the sample of width ∼0.3 mm. This spot size, which should ideally be ∼0.1 mm with the demagnification of 3/1, is limited first by the non-uniformity of the curvature of the crystal with ribs. Indeed, for a given average curvature, the crystal is more curved in the thin parts, corresponding to the gaps between ribs, than in the thick parts, corresponding to the ribs. This leads to a spreading of the focal distance along the beam axis. The effect can be seen on the image of the defocused beam on a fluorescent screen placed at the nominal focal distance: a succession of bright and dark areas with the same periodicity as ribs can be observed. The spot size is also limited by geometrical optical aberrations of the crystal. As shown by Sparks *et al.* (1980), by focusing a divergent monochromatic beam with a sagittally curved crystal, the reflectivity of the crystal vanishes on both sides of the crystal because the Bragg diffraction conditions are no longer satisfied. With a demagnification of 3/1, a maximum beam divergence of 3 mrad is achieved, and, by using Si[111] crystals, we are well inside the limits of the domain of diffraction.

The bender of the crystal is a mechanical system, shown in Fig. 5, consisting of two parallel deformable rhombs which push apart the feet of a U-shaped intermediate frame on top of which the crystal is glued. The independence of the two rhombs allows correction of an eventual conical deformation of the crystal, within the limit of the stiffness of the frame. A vertical jack on the side of the frame allows an untwisting of the crystal. Good focusing can be achieved with this system.

Crystal 2, with its bender, is put onto a three orthogonal tilt stage, γ, κ, ω, for accurate orientation adjustment. The γ rotation for tuning the Bragg diffraction conditions with respect to the first crystal has a sensitivity of $\sim$0.12 µrad per step, very small compared with the Darwin width of Si[111], for example. The tilt χ around the average beam direction allows the adjustment of the beam direction in the horizontal plane with a sensitivity of $\sim$1.4 µrad per step, which corresponds to a shift of $\sim$4 µm at the sample position with a beam at 0.2 rad incidence. The rotation ω around the normal to the crystal is used to align the cylindrical axis of the curved crystal. Ray-tracing calculations show that the misseting of this rotation, that is equivalent in a first approximation to a twist of the crystal (see below), has the effect of reducing the area of the second crystal in tune for diffraction with the first one. A 0.2° misalignment of ω reduces this area by a factor of three with Si[111] at λ = 1 Å, for example.

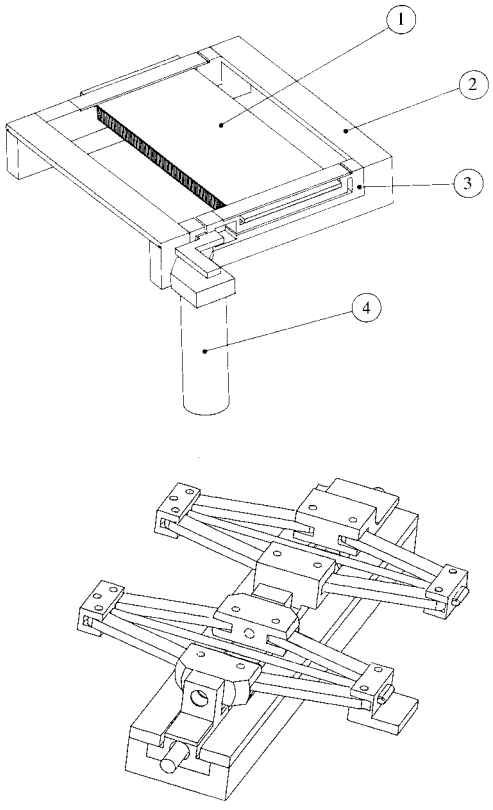

Figure 5
Bender of crystal 2 in the monochromator. Bottom: drawing of the bender showing its two independent pushing rhombs. Top: drawing of crystal 2 and crystal holder. (1) Thin silicon crystal with ribs on the back for preventing anticlastic curvature, firmly glued onto the holder; (2) U-shaped stainless-steel crystal holder which is curved, together with the crystal, by the bender which pushes aside the legs of the holder; (3) flexible part of the crystal holder allowing twist correction; (4) motorized jack acting on (3) for correcting the twist of the bent crystal.

Table 2
Geometrical data and equations of the beamline model.

Distances in the horizontal plane		
Source to sample	L	37542 mm
Source to mirror 1	x_1	26055 mm
Mirror 1 to crystal 1	L_1	1971 mm
Mirror 1 to mirror 2	L_2	3706 mm
Source to mirror 2		29762 mm
Mirror 2 to sample	x_2	7781 mm

Altitudes		
Incoming white beam	z_i	$\sim$1400 mm
Sample	z_0	$= z_i$
Mirror 1	z_i	
Mirror 2	z_0	

Equations	
Inclination of both mirrors with respect to horizontal plane	$\varphi = 0.75\varphi_c$ where $\varphi_c = a_c\lambda$, $a_c \simeq 6.85$ mrad Å^{-1} for Pt
Radius of curvature of mirror 1	$R_1 = 2x_1/\sin\varphi$
Radius of curvature of mirror 2	$R_2 = 2x_2/\sin\varphi$
Altitude difference of mirror 1 to crystal 1	$H = L_1\tan 2\varphi$
Bragg diffraction angle	$\theta_B = A\sin(\lambda/2d)$ where $2d$ = 6.271 Å for Si[111]
Angle of crystal 1 with respect to horizontal plane	$\beta = \theta_B - 2\varphi$
Distance between monochromator in and out beam	$D = L_2\sin 2\varphi + (z_i - z_0)\cos 2\varphi$
Distance between crystal 1 and 2 planes	$X = D/2\cos\theta_B$
Distance between crystal 1 and 2 normal axes	$Y = D/2\sin\theta_B$
Source to crystal 2 distance	$f_1 \simeq x_1 - X\sin\beta + Y\cos\beta$
Crystal 2 to sample distance	$f_2 = L - f_1$
Radius of curvature of crystal 2	$R_c = 2f_1f_2\sin\theta_B/(f_1 + f_2)$

2.3. *Monitors*

The beam is monitored at five different places along the beamline [(i)–(v) below]. The white-beam monitors are original and based on the observation that very thin and long W wires are heated at a temperature >1273 K if placed in the white beam because of their very high thermal resistance.

(i) *Beam altitude and vertical width of the incoming white beam.* These two parameters are monitored by a vertical beam profiler consisting of two horizontal 8 cm-long 6 µm-diameter W wires which are moved through the beam by vertical translation, while their electrical resistance is monitored.

(ii) *Imaging of the beam after reflection by the first mirror.* This monitor consists of a planar array of about 20 horizontal parallel 8 cm-long 6 µm-diameter W wires, regularly

spaced 5 mm apart from each other. The plane of the monitor is inclined in the beam at an angle of about 0.1–0.2 rad from the horizontal plane. The wires heated by the white beam emit light like glow-lamp wires, at a temperature depending on the beam intensity. The image of the beam produced in this way is observed from the top of the wire plane from the outside of the vacuum vessel through a glass window with a conventional CCD camera. The resolution of the image is about 0.1 mm and 1 mm in the vertical and horizontal directions, respectively. This type of monitoring could be improved by adding another array of wires perpendicular to the first one, and by using a colour CCD camera.

(iii) *Beam monitoring after the monochromator.* A removable fluorescent screen is used for imaging the beam just after the monochromator. This imaging is very crucial for the control of the quality of the curvature of crystal 2: misalignment, twist and conical deformation can be observed and manually corrected as explained below. The intensity of the beam is also monitored at this place by two diodes placed at the side of the beam, measuring the X-ray intensity scattered by a thin plastic foil placed in the beam. This monitor can be used for controlling the tuning of crystals 1 and 2.

(iv) *Beam monitoring at the entrance of the experimental hutch.* Same monitor as described in (iii).

(v) *Beam monitoring at the sample position.* Direct X-ray beam imaging is made with a small two-dimensional CCD camera with 10 μm resolution. The beam intensity is monitored by photomultiplier, diode or ionization chamber monitors.

3. Beamline alignment

3.1. *Beamline geometry*

Beamline alignment cannot be performed without an exact knowledge of the beamline geometry. The geometrical model and data of the beamline are described in Table 2 and Fig. 6. The absolute geometry of the beamline is defined by the altitude of the source on one end and by the altitude of the centre of the diffractometer on the other end. The height of mirrors 1 and 2 have been adjusted by telescope to be at the same altitude as the incoming beam and the diffractometer centre, respectively. Both altitudes were later refined by looking at the image of the beam cross section after reflection on the mirrors. The altitude of the mirrors is not changed during current beamline alignment.

3.2. *Beamline alignment at a given wavelength*

The standard alignment of the beamline at a given wavelength involves the following adjustments of the optical system: inclination of mirrors 1 and 2, curvature of mirrors 1 and 2, altitude of monochromator, rotation of the main monochromator axis, translations X and Y of crystal 2, and tuning of diffraction of crystal 2 with respect to crystal 1. All positions are computed using the model described in Table 2 and Fig. 6. The process of alignment is fully automated. Before setting a given motor to the calculated position, the zero switch is reset. The complete sequence of alignment can be performed in ∼5 min.

The automatic beamline alignment must be completed by a few manual adjustments. They concern mirror 2 and crystal 2. The curvature of mirror 2 sometimes needs to be optimized for minimizing the vertical size of the spot at the sample position. The inclination of mirror 2 must be adjusted accurately for centring the beam on the sample. Crystal 2 must be curved manually for obtaining the best focusing.

3.3. *Crystal 2 bending and focusing adjustment*

After having set approximately the correct average curvature, distortions and misalignment of the crystal must be eliminated. The corrections can be made following the guidelines described hereafter. Let us refer the crystal to the system of coordinates x, y, z, where x is the intersection of the plane of the uncurved crystal and the diffraction

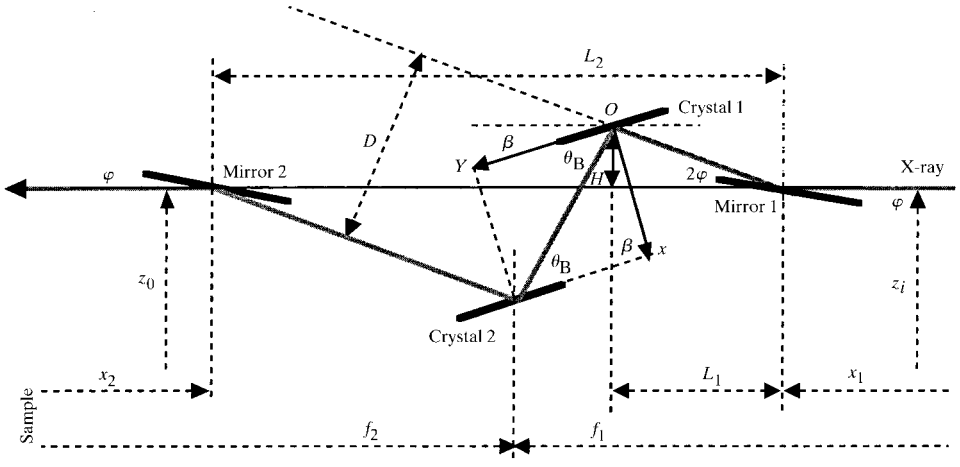

Figure 6
Geometry of the beamline model. O is the axis of the central rotation of the two-crystal monochromator, β is the central monochromator rotation angle.

plane, z is the normal to the uncurved crystal plane, and y is the transverse axis. The axis of average sagittal curvature of the crystal is parallel to x.

3.3.1. *Conical distortion*. The conical distortion can be considered as a variation of the radius of curvature of the crystal in the yz plane along the x axis (Fig. 7). The shape of the crystal with conical distortion is described by

$$z = (y^2/2R)(1 + qx/a),$$

where a is the half-length of the crystal in the x direction and q/a is the relative variation of the curvature per unit length along x. The consequence of this imperfection is a decrease of the size of the area of the crystal in tune with crystal 1. The slope of the crystal in the x direction, $\partial z/\partial x$, changes symmetrically from the centre to the edge. This imperfection is revealed by an image of the beam of the fluorescent screen of monitor 3, showing two limited diffraction areas symmetrical with respect to the beam axis (see Fig. 8). The distance between the two areas changes when the average incidence on the crystal is changed.

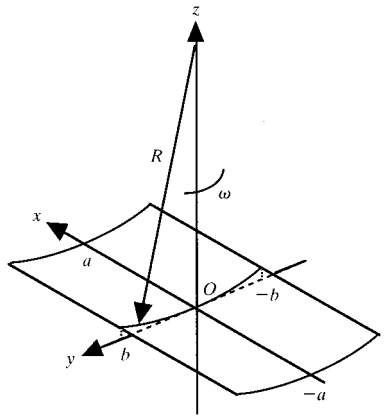

Figure 7
Diagram showing the conical distortion parameters.

3.3.2. *Twist and ω rotation*. The second and third defects to be corrected are the twist of the crystal along the y axis and the misalignment of the cylinder axis of the curved crystal with respect to x. The equation of the twisted curved crystal is given by

$$z = (y^2/2R) + (pxy/b),$$

where b is the half-width of the crystal in the y direction and p and $-p$ are the slopes $\partial z/\partial x$ of the crystal at the two edges $y = \pm b$, which define the amplitude of the twist. In other words, p/b is the variation per unit of length in the y direction of the angle of incidence of the beam.

The equation of the crystal rotated by ω around the z axis is given by

$$z = (y\cos\omega + x\sin\omega)^2/2R.$$

These two equations show that, to a first approximation, the twist of the crystal is equivalent to a misalignment of the cylinder axis by a rotation ω given by

$$\omega = Rp/b.$$

This equivalence between twist and ω rotation can be used for achieving a fast and efficient point focusing of the beam. At higher-order approximation, both defects are never-

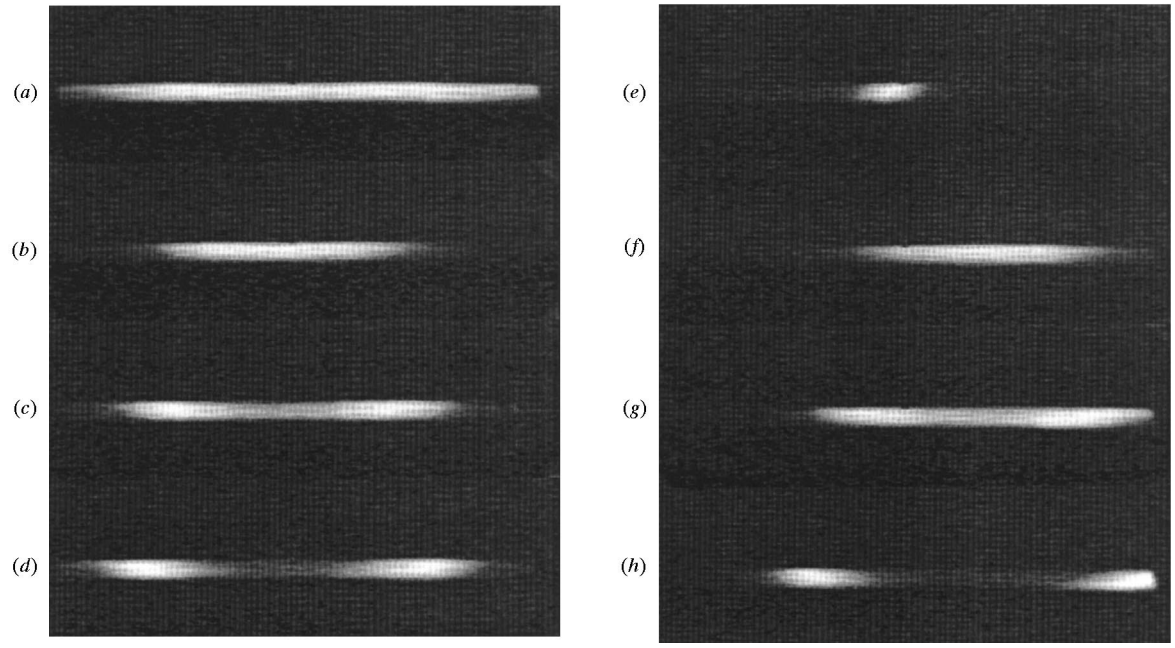

Figure 8
Cross-section views of the monochromated beam given by the fluorescent screen installed just after crystal 2 of the monochromator. (*a*) Standard view of the beam after crystal 2 curvature optimization. (*b*), (*c*), (*d*) Crystal with conical deformation observed at three distinct values of the tuning angle: the diffracting area is split into two symmetrical parts. (*e*) Crystal with a strong twist deformation. (*f*), (*g*), (*h*) Crystal with both defects (conicity and twist) observed at three distinct values of the tuning angle. The diffracting area is split into two asymmetrical parts observed.

theless not equivalent. A well focused spot may still show low-intensity wings due to residual optical aberrations. For reducing these aberrations it is necessary to correct both defects independently. This is necessary for small-angle scattering experiments where the beam collimation is achieved with a multislits system. In that case, the low-intensity side beam, when hitting the antiscattering slits located near the sample, produces a high background at small angles. Twist and misalignment are revealed on the fluorescent screen by a limited asymmetrical image of the beam. The limited diffraction area on crystal 2 goes from one side of the crystal to the other when the crystal is rotated (see Fig. 8).

Conicity, twist and misalignment produce a decrease in the reflected intensity. As a consequence, the intensity is no longer proportional to the horizontal beam divergence. The width δy of the limited area which diffracts the beam is given by

$$\delta y = aR\omega_D/qy \qquad \text{and} \qquad \delta y = b\omega_D/p$$

for conicity and twist, respectively, as a function of the Darwin width ω_D.

The observation of the characteristic alterations of the image of the beam produced by these imperfections and of their modifications by changing the tuning of crystal 2 with respect to crystal 1 is the basic method for manually correcting these distortions (see Fig. 8). With a quantitative analysis of these images and with the help of the above equations, it will be possible in the near future to automatize these corrections (Ferrer, 1998).

The effect of the thermal curvature of crystal 1 can also be observed on the image of the beam on the fluorescent screen. It is basically characterized by the narrowing of the image in the x direction and by the shift of the image along this axis when the crystal tuning is changed.

4. Results and discussion

The three major requisites for a good beamline dedicated to anomalous multiwavelength diffraction experiments are (i) a simple, fast and safe procedure for operating large-scale wavelength changes involving beamline realignment, (ii) a robust monochromator for very fast high-resolution highly reproducible small-scale energy changes, without beamline realignment, and (iii) high intensity.

The beamline realignment technique has already been discussed above. The control of the focusing of crystal 2 has still to be improved on D2AM for meeting the first goal. The second goal, on the contrary, has been achieved. For small-scale energy changes, the monochromator is operated in the so-called channel-cut mode where only the central rotation is moved, to the exclusion of any other crystal setting. The energy range which can be scanned in this mode, without important loss of intensity on both sides of the range, is typically of the order $\pm 10\%$ of the average energy. The limitation of this energy range does not come so much from the defocusing of the beam accompanying the variation of the angle of incidence of the beam on crystal 2 (which should produce a theoretical decrease of intensity on a sample smaller than the beam, of about 10 to 20%), but from an eventual horizontal shift of the beam due to slight residual misalignment of the crystal or from a default of alignment of the diffractometer with respect to the beam axis.

The quality of the monochromator is illustrated in Fig. 9, showing the measured transmission of Ga at the K absorption edge: the f'' white line is well resolved and the stability of the baseline allows one to perform diffraction anomalous fine-structure (DAFS) experiments or X-ray absorption fine-structure (XAFS) experiments over a wide range of energy. The stability of the monochromator is demonstrated in Figs. 10 and 11. In Fig. 10, the result of repeated measurements of the fluorescence of a Pt sample at the Pt absorption edge over several hours is shown. The reproducibility of the energy setting is of the order of 0.5 eV. The thermal stability is shown in Fig. 11: after a

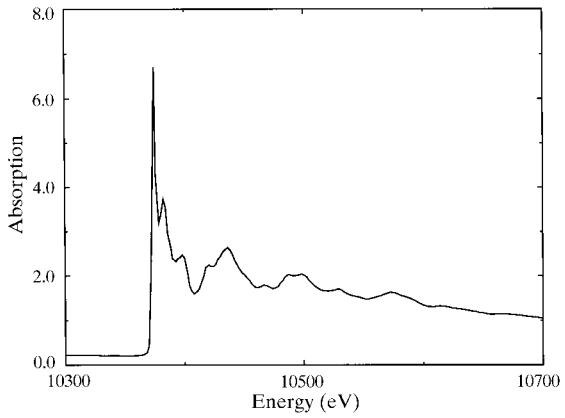

Figure 9
Absorption edge of Ga, at E = 10368 eV, measured by transmission on D2AM with 1 eV steps.

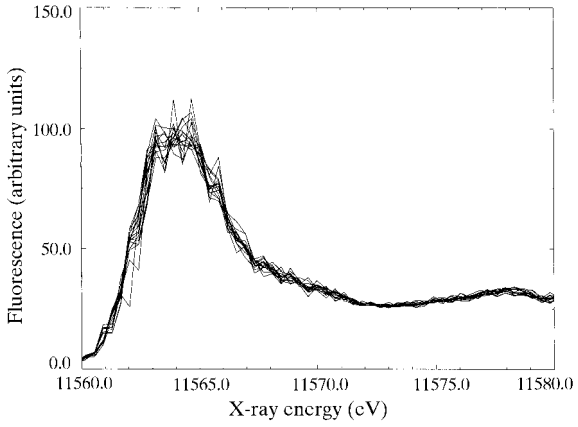

Figure 10
Repeated fluorescence scans of a Pt metal foil over several hours at the Pt absorption edge, E = 11562 eV, with the D2AM monochromator. The dispersion of the curves in abscissa corresponds to 0.5 eV. The fluorescence intensity is given in arbitrary units.

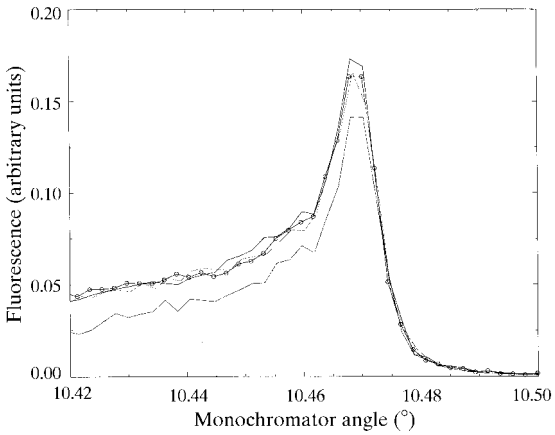

Figure 11
Fluorescence scans of a W metal foil at the W absorption edge, E = 10200 eV, before (circles) and after a shutdown of the beam of 15 min. The lowest curve was measured immediately after the beam shutter reopening, the two others 5 and 10 min later. Fluorescence in arbitrary units.

beam shutdown, no shift of wavelength is found and only 5–10 min are necessary for recovering the initial intensity.

4.1. *Future improvements*

The limitations of the beamline are presently the following.

(i) The highest intensity is obtained between 0.9 Å and 1.3 Å. It has been nevertheless possible to undertake very good experiments at the absorption edges of Fe (K edge, $\lambda \simeq 1.74346$ Å), Cr (K edge, $\lambda \simeq 2.0702$ Å) or Pr (L_{III} edge, $\lambda \simeq 2.0791$ Å). Below 0.9 Å there is a rapid decrease in the intensity which is due to the fact that Si[111] crystals are not well adapted to very short wavelength monochromatization because the angle of incidence become very low. This produces a decrease in the intensity, firstly by diminution of the vertical acceptance of the crystals and secondly by the relative increase of the effect of the thermal curvature of crystal 1. Consequently, for keeping high intensity down to 0.5 Å, for example, it will be necessary to use higher-order reflections from Si crystals like [220] or [311] and improve the technique of cooling crystal 1 to reduce its thermal curvature.

(ii) The horizontal focusing of the beam by sagittal curvature of crystal 2 should be improved. By using a bending device less sensitive to mechanical imperfections than the present bender, the bending of the crystal could be made more reproducible, a condition required for the automatization of the operation. A technique for sagittal bending of the crystal with negligible anticlastic curvature, but not based on the use of ribs on the back of the crystal, should produce a factor of two increase in intensity.

Two developments are therefore presently foreseen: (i) using cryo-cooling on the first monochromator crystal and (ii) using piezoelectric actuators for bending a long U-shaped crystal (Thomas & Vettier, 1993). The first improvement will allow one to extend the range of accessible X-ray photon energy up to 25 keV, and the second improvement should make faster and more efficient the focusing of the beam by sagittal bending. These improvements are going to be tested and implemented on the new french CRG beamline FIP for biological macromolecular crystallography, which is under construction at front-end BM30.

The design and the construction of the beamline benefited from the contribution of many people. Ian Kilvington, Paul Berkvens, Pierre Taunier, Philippe Jeantet, Jean-Paul Roux, Lionel Mallet, Frédéric Livet, Françoize Bley, Eric Geissler, Anne-Marie Hecht and Marie-Claire Saint-Lager provided significant help to this achievement which is gratefully appreciated. The silicon mirrors were made by REOSC (Massy, France), the mechanics of the mirrors by IRELEC (Grenoble, France) and the mechanics of the monochromator by MICROCONTROLE (Evry, France). The project was realized with the support of the following organizations in France: Région Rhône-Alpes, Département de l'Isère, Ministère de l'Education Nationale, de l'Enseignement Supérieur et de la Recherche, Commissariat à l'Energie Atomique (CEA), Centre National de la Recherche Scientifique (CNRS). The operation costs of the beamline are jointly equally supported by the CEA and the CNRS.

References

ANSYS (1991). Swanson Analysis Systems Inc., Houston, PA, USA.
Bilderback, D. H. (1981). *Proc. SPIE*, **315**, 90–102.
Ferrer, J.-L. (1998). Submitted.
Ferrer, J.-L., Roth, M. & Fanchon, E. (1995). *Rev. Sci. Instrum.* **66**, 2089–2091.
Hendrickson, W. A., Smith, J. L., Phizackerley, R. P. & Merritt, E. A. (1988). *Proteins Struct. Funct. Genet.* **4**, 77–88.
James, R. W. (1982). *The Optical Principles of the Diffraction of X-rays*, p. 173. Woodbridge, Connecticut: Ox Bow.
Roth, M., Ferrer, J.-L., Simon, J.-P. & Geissler, E. (1992). *Rev. Sci. Instrum.* **63**, 1043–1046.
Simon, J.-P., Geissler, E., Hecht, A.-M., Bley, F., Livet, F., Roth, M., Ferrer, J.-L., Fanchon, E., Cohen-Addad, C. & Thierry, J.-C. (1992). *Rev. Sci. Instrum.* **63**, 1051–1054.
Sparks, C. J., Borie, B. S. & Hastings, J. B. (1980). *Nucl. Instrum. Methods*, **172**, 237–242.
Sparks, C. J., Ice, G. E., Wong, J. & Batterman, B. W. (1982). *Nucl. Instrum. Methods*, **194**, 73–78.
Thomas, M. & Vettier, C. (1993). ESRF-ILL Internal Report. ESRF, Grenoble, France.